Hierarchical Conjugate Structure of γ-Fe_2O_3 Nanoparticles and PbSe Quantum Dots for Biological Applications

Lioz Etgar,[†] Efrat Lifshitz,[‡] and Rina Tannenbaum*[,§,||]

Nanoscience and Nanotechnology Program, Schulich Faculty of Chemistry, and Department of Chemical Engineering, and Russell Berrie Nanotechnology Institute, Technion-Israel Institute of Technology, and School of Materials Science and Engineering, Georgia Institute of Technology, Atlanta, Georgia

Received: January 8, 2007; In Final Form: February 28, 2007

The development and characterization of a unique conjugated structure comprised of γ-Fe_2O_3 nanoparticles (NPs) and PbSe nanocrystal quantum dots (NQDs), bonded via chemical functional groups, are discussed. Compatibility with an aqueous environment was rendered by exchanging the traditional organic surfactants (oleic acid) of the PbSe NQDs and γ-Fe_2O_3 NPs with 2-aminoethanethiol and polyhedral silsesquioxane hydrate octakis ligands, respectively. Comparison of the transmission electron microscopy (TEM) images of the PbSe NQDs and γ-Fe_2O_3 NPs capped with either organic or water-soluble ligands highlights the preservation of the morphology and size of both types of nanoclusters upon ligand exchange. Furthermore, the absorbance, photoluminescence (PL), and Fourier transform infrared spectra of the PbSe QDs revealed that the optical properties of the NQDs were retained during the surfactant exchange. High-resolution TEM images of the complete conjugated structure validate the presence of the coupling between the PbSe NQDs and the γ-Fe_2O_3 NPs. This unique system has substantial advantages for biological applications such as bio-sensing, detection of cancer cells, and drug delivery.

1. Introduction

Semiconductor nanocrystal quantum dots (NQDs) and magnetic metal oxide nanoparticles (NPs) possess unique properties not encountered in the corresponding bulk materials.[1−7] The formation of NQD−NP conjugated structures should have a scientific and technological merit in harvesting the special optical and magnetic properties of their constituents and thus can be utilized in new and emerging technologies such as magnetic transport, separation and fluorescence tagging of cancer cells, and bacteria or virus studies.[8−20] This paper reports the development and characterization of superparamagnetic γ-Fe_2O_3 nanoparticles (NPs) and PbSe nanocrystalline quantum dots (NQD), capped with molecular ligands, bonded via functional groups and dissolved in aqueous solutions, designed to be compatible with biological and medical applications.

The NQDs exhibit characteristic electronic and optical tunability with the variation of their size. PbSe NQDs constitute the focus of extensive attention due to some unique intrinsic properties.[21−23] Bulk PbSe material have a cubic (rock salt) crystal structure and a narrow direct band gap (0.28 eV at 300 K), 4-fold degenerated at the L point of the Brillouin zone. The high dielectric constant ($\epsilon_\infty = 24.0$) and the small electron and hole effective mass ($0.1m_0$) create an exciton with a relatively large effective Bohr radius (46 nm). Inter-band optical studies of colloidal PbSe NQDs exhibit well-defined band-edge excitonic transitions tuned between 0.3 and 1.1 eV, relatively large ground-state cross sections of absorption ($\sim 10^{-16} - 10^{-15}$ cm^{-2}), long excitonic lifetimes ($\sim$200−800 ns), and exceptionally high quantum efficiencies of the luminescence (80%).[24−27] Recently, amplified spontaneous emission from PbSe NQDs was demonstrated, with relatively large gain parameters.[28,29] Furthermore, impact ionization obtained by photoexcitation with $h\nu > 3E_g$ and its competition with Auger recombination has been discussed.[30] These unique properties indicate the potential applicability of the PbSe NQDs in telecommunications, eye-safe lasers, solar cells, electroluminescence devices, and biological markers.[31−33]

Iron oxide nanoparticles have physical and chemical properties that are characteristic of neither the molecular nor the bulk counterparts.[34,35] Quantum size effects and the large surface area of magnetic nanoparticles dramatically change some of the magnetic properties and exhibit superparamagnetic phenomena and quantum tunneling of magnetization because each particle can be considered as a single magnetic domain. On the basis of their unique mesoscopic physical, tribological, thermal, and mechanical properties, superparamagnetic nanoparticles offer a high potential for several applications in different areas such as ferrofuids, color imaging, magnetic refrigeration, detoxification of biological fluids, magnetically controlled transport of anti-cancer drugs, magnetic resonance imaging contrast enhancement, and magnetic cell separation.[36−39]

The present paper discusses the preparation and characterization of the PbSe NQDs−γ-Fe_2O_3 NPs conjugated structure. The main challenge in the utilization of the NQD constituents as fluorescent probes and NPs as magnetically controlled transport platforms in biological applications is the concern regarding their compatibility with the biological environment (i.e., whether they have the ability to maintain their dispersion and their properties in aqueous media). Previous efforts to prepare the NQDs and the magnetic NPs in aqueous media were met with serious

* Corresponding author. E-mail: rinatan@technion.ac.il or rinatan@mse.gatech.edu.

[†] Nanoscience and Nanotechnology Program, Technion-Israel Institute of Technology.

[‡] Schulich Faculty of Chemistry, Technion-Israel Institute of Technology.

[§] Department of Chemical Engineering, and Russell Berrie Nanotechnology Institute, Technion-Israel Institute of Technology.

[||] Georgia Institute of Technology.

10.1021/jp070157e CCC: $37.00
Published on Web 04/05/2007

SCHEME 1: Chemical Structures of Three Different Capping Ligands: OA, AET, and PSS, and Their 3-D Space-Filling Model Structures

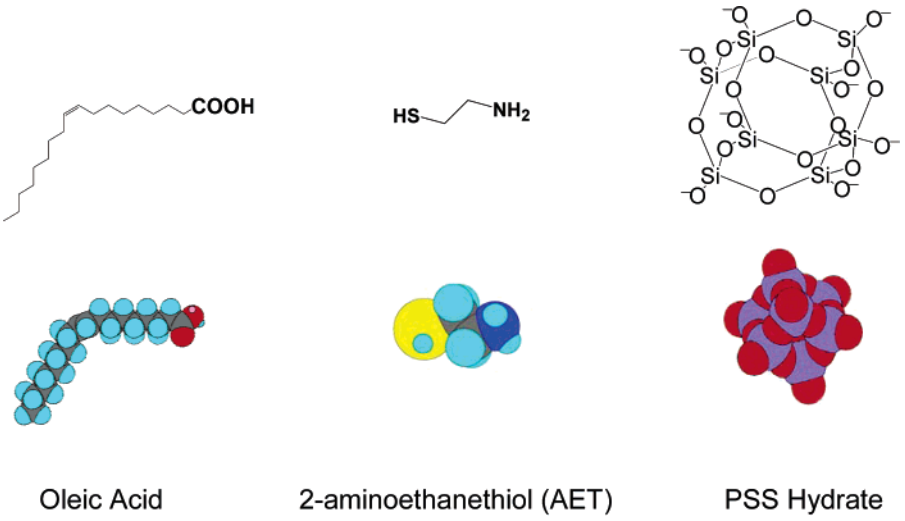

SCHEME 2: Schematic Representation of Ligand Exchange Process and Transfer of Nanoparticles from Organic Phase to Aqueous Phase[a]

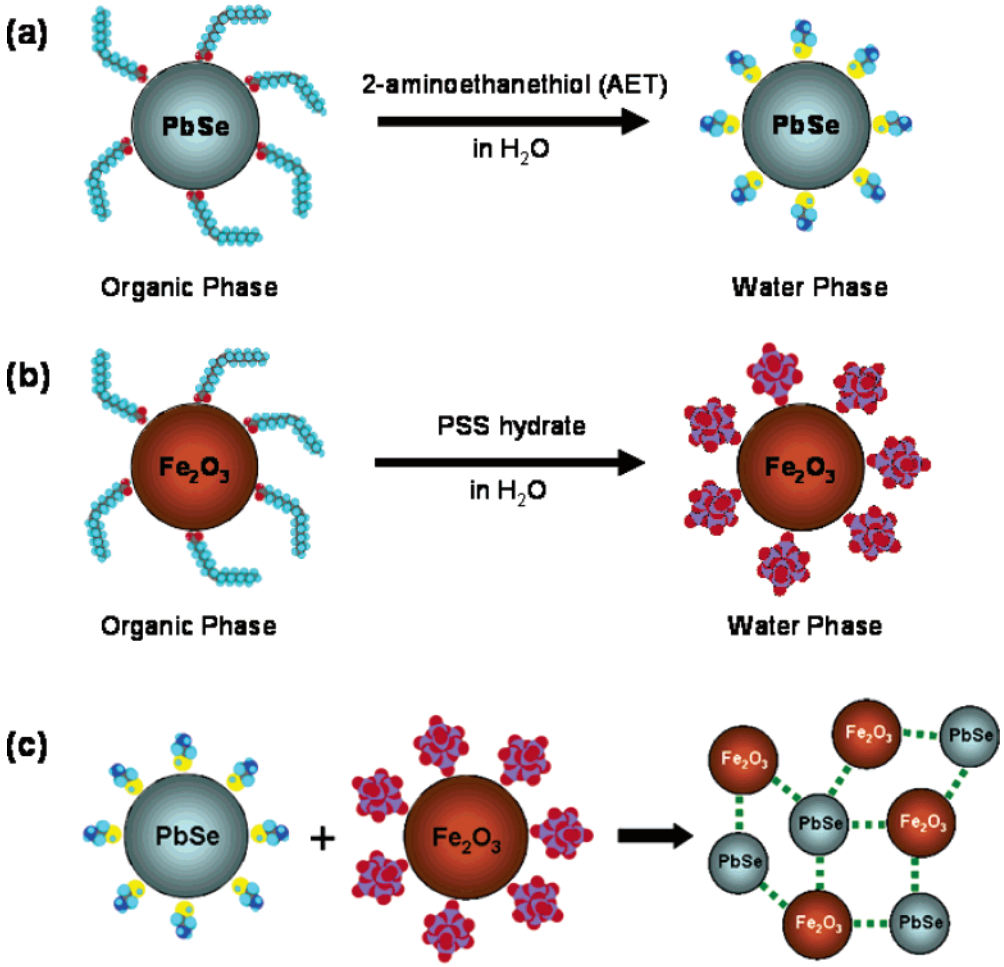

[a] (a) Transfer of PbSe NQDs by exchange of OA ligand with water-soluble AET surfactant. (b) Transfer of γ-Fe_2O_3 NPs by exchange of OA ligand with water-soluble PSS hydrate octakis surfactant. (c) Coupling between γ-Fe_2O_3 NPs and PbSe NQDs to form the conjugated, hierarchical structures.

obstacles associated with chemical stability and particle dispersion.[40] This work concentrates on a novel, alternative procedure, based on the initial preparation of the nanoparticles by traditional synthesis and capping methods with organic stabilizers, followed by a carefully tailored exchange of the surfactants with selective water-soluble ligands. Furthermore, given the hierarchical design approach taken in this work, these water-soluble ligands (e.g., 2-aminoethanethiol (AET) and polyhedral silsesquioxane (PSS) hydrate octakis) were chosen to include specific functional groups that would enable the subsequent chemical bonding

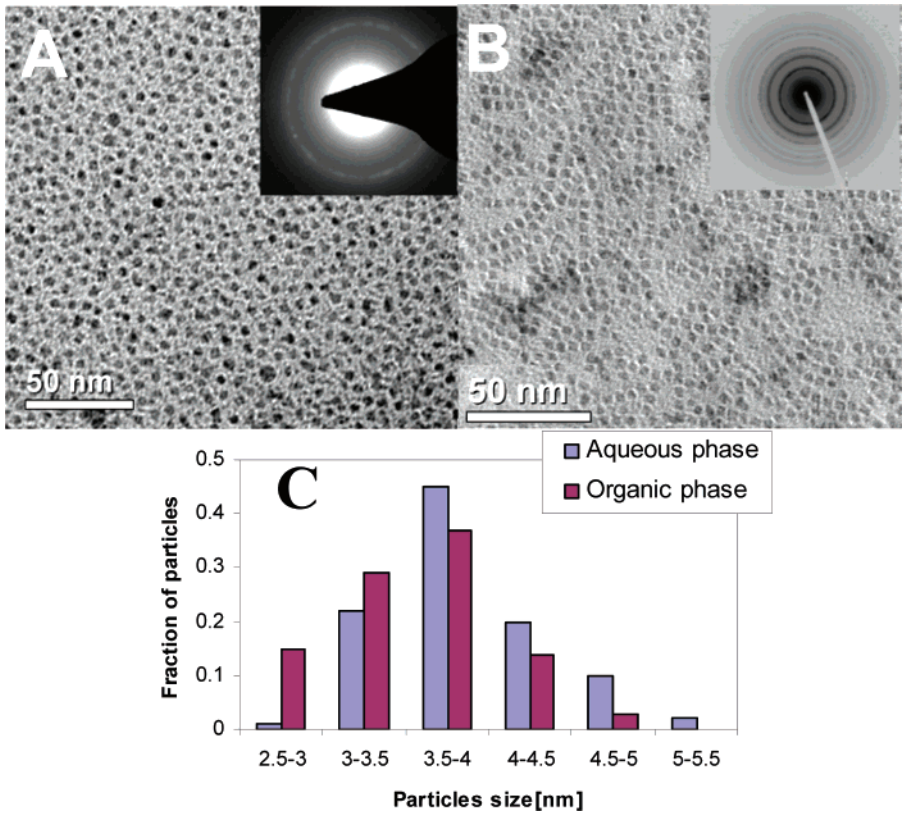

Figure 1. TEM images of PbSe NQDs: (A) Capped with OA/TOP ligands in an organic medium. (B) Capped with the AET ligand in an aqueous medium. The insets in panels A and B represent the corresponding electron diffraction patterns. (C) Histogram of the size distribution of the capped NQDs in the organic and aqueous media.

between NQDs and NPs in aqueous solutions. The structural and morphological properties of the constituents and the conjugated structures were examined by transmission electron microscopy (TEM), while their optical properties were characterized by absorption, photoluminescence (PL), and Fourier transform infrared (FTIR) spectroscopy.

2. Experimental Procedures

2.1. Materials. 2-Aminoethanethiol (AET) ligands (AET 98%, 97+ % purity), methanol (CH_3OH, Aldrich, d = 0.79 g/cm^3, bp 65 °C), and chloroform ($CHCl_3$, spectroanalytical grade 99%, d = 1.48 g/cm^3, bp 62 °C) are commercially available products and were purchased from Aldrich.

Polyhedral silsesquioxane (PSS) hydrate octakis(tetramethylammonium) ($C_{32}H_{96}N_8O_{20}Si_8 \cdot xH_2O$, mp 135−143 °C) and hexane (C_6H_{14}, d = 0.659 g/cm^3, bp 69 °C) are commercially available products and were also purchased from Aldrich.

Lead acetate trihydrate (Pb-Ac, $Pb[CH_3COO]_2 \cdot 3H_2O$, GR) was purchased from Merck. PhEt ($C_6H_5OC_6H_5$, 99%,), oleic acid (OA, $CH_3(CH_2)_7CHCH(CH_2)_7COOH$, 99.8%), trioctylphosphine (TOP, $(C_8H_{17})_3P$), selenium (Se, 99.995% purity), iron pentacarbonyl ($Fe(CO)_5$, 99.999% purity), octyl ether ($(CH_3(CH_2)_7)_2O$, 99% purity, d = 0.806 g/cm^3, bp 286 °C), and ethanol (CH_3CH_2OH, 99.5% purity, d = 0.789 g/cm^3, bp 78 °C) were all purchased from Aldrich. Scheme 1 shows the chemical formulae of all three ligands: OA, AET, and PSS, together with their space-filling models.

2.2. Synthesis of PbSe NQDs and Fe_2O_3 NPs. *2.2.1. Synthesis of Organically Capped and Water-Soluble PbSe NQDs.* The synthesis of the PbSe NQD core covered with organic surfactant followed a modified procedure reported earlier[41] and included the following stages: (1) 0.71 g of lead acetate trihydrate [Pb-AC] was dissolved in a solution that was composed of 2 mL of PhEt, 1.5 mL of oleic acid, and 8 mL of trioctylphosphine, under standard inert conditions in the glove box, and was inserted into a three-necked flask (flask I) ; (2) 10 mL of PhEt was inserted into a three-necked flask (flask II) under inert conditions of the glove box; (3) both flasks were taken out of the glove box and were placed on a Schlenk line and heated under a vacuum to 100−120 °C for an hour; (4) flask I was cooled to 45 °C, while flask II was heated to 180−210 °C, both under a stream of argon gas; (5) 0.155 g of selenium powder was dissolved in 2.0 mL of TOP, forming a TOP/Se solution, under standard inert conditions of a glove box; then, 1.7 mL of this solution was injected into flask I on the Schlenk line; and (6) the contents of flask I, containing the reaction precursors, were injected rapidly into the PhEt solution in flask II, reducing its temperature to 100−130 °C, leading to the formation of PbSe QDs within the first 15 min of the reaction. The procedure described produced nearly monodispersed NQDs with a <5% size distribution, and an average size between 3 and 9 nm, controlled by the temperature and by the duration of the reaction.

To create water-soluble PbSe NQDs with a positively charged capping, 100 μL of an organically capped PbSe NQD solution was dissolved in 5 mL of chloroform. Subsequently, 100 μL of a 0.5 M methanol solution of AET was added. The relatively stronger affinity of the thiol group originating from AET ($HS(CH_2)_2NH_3$) ligands to the PbSe surface, with respect to that of the oleic acid carboxyl group, led to a ligand exchange, as shown schematically in Scheme 2a. Thus, the exterior surfaces of the PbSe NQDs exchanged aliphatic terminating groups (the CH_3 end-groups of the oleic acid) with the amine groups of the AET ligands. This immediately caused flocculation of the PbSe NQDs in chloroform. Subsequently, 5 mL of water was added to the suspension, resulting in a separation of the mixer into

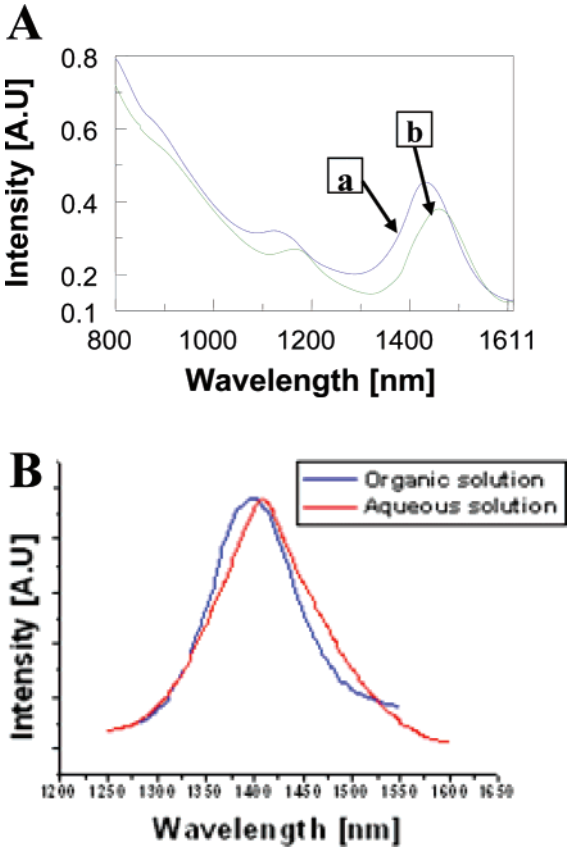

Figure 2. Spectroscopic properties of the PbSe QDs in an organic solvent and in an aqueous medium following the ligand exchage. (A) Absorbance spectra of PbSe NQDs capped with organic ligand (a) and water-soluble (AET) ligands (b). (B) PL spectra of the organically capped and water-soluble PbSe NQDs showing a bright $1S_h-1S_e$ exciton transition with a fwhm of 105.91.

two phases (water above chloroform). Upon further shaking, the flocculated NQDs dissolved into the water phase and formed a clear suspension.

2.2.2. Synthesis of Organically Capped and Water-Soluble γ-Fe_2O_3 Magnetic NPs. The synthesis of γ-Fe_2O_3 NPs covered with organic surfactant followed a modified procedure to that documented by Held et al.[42] A total of 0.2 mL of $Fe(CO)_5$ (1.52 mmol) was added to a mixture containing 10 mL of octyl ether and 1.28 g of oleic acid (4.56 mmol) at 100 °C. The resulting mixture was heated to 300 °C and kept at that temperature for 1 h. During this time, the initial orange color of the solution gradually changed to black. The resulting black solution was cooled to room temperature and centrifuged. The precipitate was removed, the remaining supernatant solution was then collected, and ethanol was added to produce reversible flocculation of the NPs. The solution was centrifuged again, and the precipitate was saved and subsequently suspended in hexane to produce a suspension of 5 nm iron NPs. Exposing this suspension to air for several days resulted in the complete oxidation of the iron NPs into dispersed 5 nm γ-Fe_2O_3 NPs.

The mentioned γ-Fe_2O_3 NPs were transferred into a water-soluble solution, using the procedure documented by Rotello et al.[43] A total of 10 mg of iron oxide NPs was dissolved in 2 mL of hexane, and 100 mg of PSS hydrate octakis was dissolved in 2 mL of water. These solutions were mixed to a solute weight ratio of 10:1. The structure of the PSS hydrate octakis ($C_{32}H_{96}N_8O_{20}Si_8 \cdot xH_2O$) molecules is an octahedral shape featuring eight siloxy groups; therefore, the resulting water-soluble γ-Fe_2O_3 NPs was capped by a negative charge, as shown

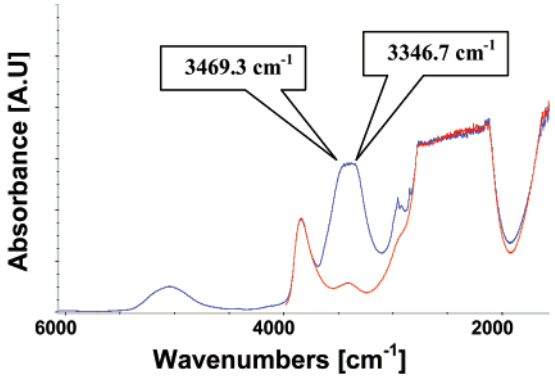

Figure 3. FTIR spectra of the OA-capped PbSe NQDs (red line) and AET-capped, water-soluble PbSe NQDs (blue line).

schematically in Scheme 2b. This bilayer system stayed under an inert environment for 2−3 min and was stirred rapidly for 24 h, during which the NPs were transferred to the aqueous phase. The solution phases were carefully separated, and the water-soluble iron oxide NPs were run through a 0.22 μm filter.

2.2.3. Coupling between PbSe QDs and γ-Fe_2O_3 NPs in an Aqueous Medium. The coupling process leading to the formation of the conjugate structures of γ-Fe_2O_3 nanoparticles and PbSe quantum dots was straightforward. It involved a simple mixing of equal volumes of the water-based solutions of the AET-capped PbSe quantum dots with a water-based solution of the PSS-capped γ-Fe_2O_3 nanoparticles, as shown in Scheme 2c. No clouding of the solution was observed during the mixing process, and the resulting solution remained clear.

2.3. Characterization of PbSe NQDs and γ-Fe_2O_3 NPs in Both Organic and Aqueous Media. A Jasco V-570 UV−vis/NIR spectrophotometer was used to obtain the absorption of the PbSe NQDs. The PL spectra were obtained by exciting the samples with a Ti:sapphire laser, while emission was recorded using an Acton monochromator equipped with a cooled Ge detector. All measurements were carried out at room temperature. The PL quantum efficiency (QE) was measured utilizing an integrating sphere technique described by Friend et al.[44] A solution of NQDs was placed inside an integrating sphere (Labsphere, Inc. IS-040-SL with UV−vis/NIR reflectance coating) and was excited by monochromatic light (Xenon lamp, fiber coupled to a monochromator). The PL spectra were detected using a fiber coupled spectrometer equipped with a liquid nitrogen-cooled Ge photodetector, with lock-in amplification. The entire system response was normalized against a calibrated detector, and care was taken to ensure that the sample absorption was above 20%. The TEM micrographs were taken by a Technai T12 transmission electron microscope operating at 120 kV with a magnification of 52 000. The high resolution transmission electron microscopy (HRTEM) micrographs were recorded with a Jeol 4000EX instrument operating at 400 kV with a magnification of 200 000. The FTIR spectra of thoroughly washed and dried samples were measured on a Nicolet Nexxus 8700 infrared spectrophotometer. The spectra were collected at a resolution of 4 cm^{-1} with 50 scans per spectrum.

3. Results and Discussion

3.1. Synthesis and Characterization of Water-Soluble PbSe NQDs. Figure 1A shows the TEM images of PbSe NQDs capped with OA/TOP and suspended in chloroform solution. Figure 1B shows the corresponding PbSe NQDs after the ligand exchange with AET and suspended in water. Comparison between the two images suggests that the size, shape, and

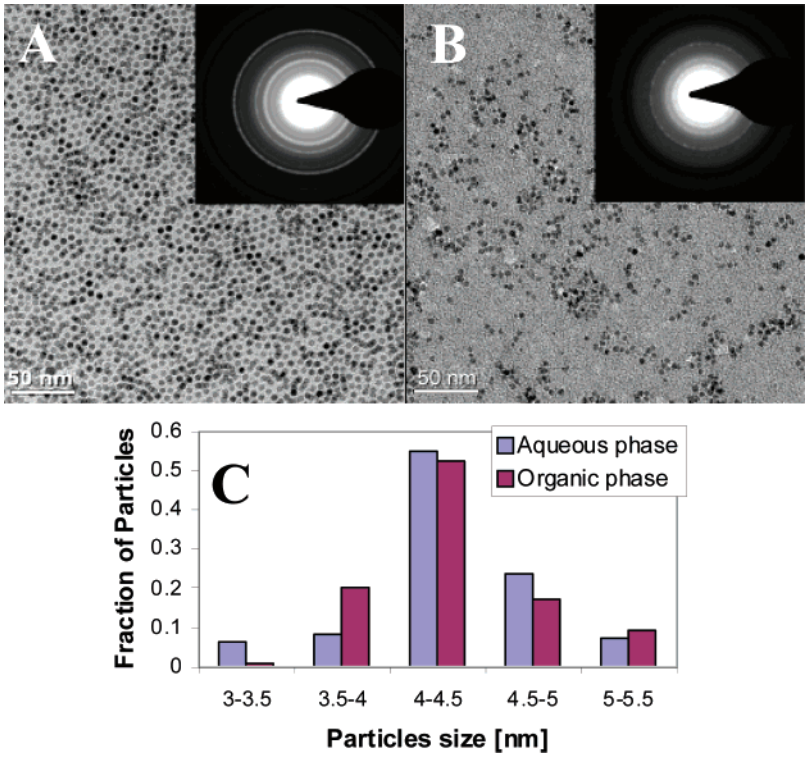

Figure 4. TEM images and electron diffraction (insets) of γ-Fe_2O_3 NPs. (A) Capped with OA ligands and suspended in a hexane solution. (B) Capped with PSS hydrate octakis ligands and suspended in an aqueous solution. (C) Histograms of the size distributions of the γ-Fe_2O_3 NPs shown in panels A and B. Average size of the NPs in hexane is 4.31 ± 0.03 nm and in the aqueous suspension is 4.33 ± 0.046 nm.

disparity of the NQDs before and after the ligand exchange have not been altered by the process. Furthermore, the water-soluble NQDs exhibited a high chemical stability under a nitrogen atmosphere for an extended period of time (over months), without any indication of aggregation or photodegradation. The electron diffraction pattern of the PbSe NQDs sample in the aqueous medium (Figure 1B inset) confirms that the NQDs have a perfect cubic close-packed (ccp/fcc) crystal structure with excellent agreement with the cubic (rock salt) structure of bulk PbSe.[40] Analysis of the size distribution of the synthesiszed PbSe NQDs, based on the TEM image, is shown in Figure 1C. The average size of the PbSe NQDs in the organic medium was 4.01 ± 0.05 nm, and in the aqueous medium, it is 3.90 ± 0.043 nm, suggesting that the average size of the NQDs varied only by a small percent upon the ligand exchange.

The absorbance spectra of the organically capped PbSe NQDs with OA and TOP ligands and the water-soluble, AET-capped PbSe NQDs are shown in Figure 2A. The spectra of these NQDs exhibit pronounced excitonic transitions with the lowest energy exciton ($1S_h-1S_e$) centered around 1440 nm. Comparison between the absorbance curves, and in particular the transition energies and the full width at half-maximum (fwhm), reveals that as a result of the ligand exchange process, the size, quantum confinement, and crystalline quality of the NQDs were not altered. The PL spectra of the OA/TOP-capped and AET-capped PbSe NQDs are given in Figure 2B. Both spectra consist of an intense single band with a fwhm of ~100 nm, further confirming that the high-quality optical properties of the PbSe NQDs were not affected by the ligand exchange process. The PbSe NQDs have electronic states that are mostly p-like, and hence, the surfaces do not create localized states in the gap.[45] This could explain the fact that the PL QE of the PbSe NQDs in the aqueous solution is 25%, while the QE of the PbSe NQDs in organic medium has been reported to reach 40%.[41] Furthermore, the calculated absorption cross section is $10^{-16}-10^{-15}$ cm^2, which

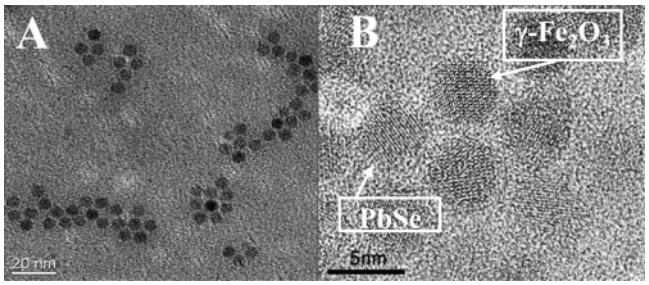

Figure 5. (A) TEM image of the magnetic γ-Fe_2O_3 NPs and semiconductor PbSe NQDs conjugated ensemble. (B) High-resolution TEM image of a small domain of the conjugated ensemble shown in panel A. Panel B reveals the existence of two types of particles, the γ-Fe_2O_3 NPs and PbSe NQDs, with different crystallographic fringes.

also indicates that the properties of the PbSe NQDs do not change by the ligand exchange, and thus, the water-soluble NQDs potentially can be used as biological fluorescing tags.

Figure 3 shows the FTIR spectra of the organically capped PbSe NQDs in the organic solution and the corresponding AET-capped NQDs in the aqueous solution. The FTIR curve of the water-soluble NQDs exhibits two distinct bands, centered at 3469.3 and at 3346.7 cm^{-1}, corresponding to the asymmetric and symmetric stretching vibrations of the terminal N−H bonds of the free primary amine group, respectively.[46] Thus, these bands reveal the existence of the amine-containing stabilizing molecules adsorbed on the surface NQDs. As will be discussed next, these amine functional groups will be accessible for further bonding with the stabilized iron oxide NPs.

3.2. Synthesis and Characterization of Water-Soluble γ-Fe_2O_3 NPs. Previous studies have shown that the decomposition of $Fe(CO)_5$ in hydrocarbon solvents under an inert atmosphere in the presence of various stabilizing ligands provides a simple and effective method to prepare highly monodisperse zero-valent magnetic iron NPs,[47−50] while their

SCHEME 3: Chemical Interactions between γ-Fe_2O_3 NPs and PbSe NQDs via Hydrogen Bonding of AET and PSS Ligands[a]

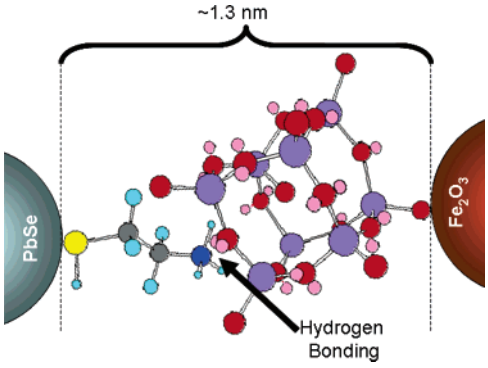

[a] Hydrogen bonding lowers the energy of the system from 1077 to 699 kcal/mol. Energy minimization calculations were performed with Gaussian 98[53] and rendered by ChemDraw[54] 3-D commercial software.

exposure to ambient atmosphere resulted in the formation of various types of monodisperse, highly crystalline iron oxide nanoparticles, such as maghemite, Fe_2O_3. The thermal decomposition of $Fe(CO)_5$ under ambient conditions resulted in the almost exclusive formation of magnetic γ-Fe_2O_3 NPs. These capped γ-Fe_2O_3 NPs were transferred into an aqueous solution by exchanging their stabilizing surfactants with PSS hydrate octakis molecules as shown in Scheme 2b. Figure 4A,B represents the TEM images of the γ-Fe_2O_3 NPs before and after the ligand exchange. These images highlight the fact that the PSS hydrate octakis-coated NPs remain discrete and that their core size is unchanged. In addition, these images indicate that no degradation takes place upon the transfer from the organic to the aqueous environment. Figure 4A shows maghemite NPs stabilized with oleic acid and dispersed in a hexane solution. The ligands exchanged from oleic acid in hexane to PSS hydrate octakis in water ensured the continued stabilization and dispersion of the NPs in the aqueous medium (Figure 4B). The electron diffraction pattern of the γ-Fe_2O_3 NPs in the organic medium and in the aqueous solution (insets in Figure 4A,B, respectively) confirms that the magnetic NPs retain their γ-Fe_2O_3 structure. Analysis of the average size and size distribution of the NPs based on the TEM images is shown in Figure 4C. The average size of the γ-Fe_2O_3 NPs in the organic medium is 4.31 $\pm$ 0.03 nm, and in the aqueous medium, it is 4.33 $\pm$ 0.046 nm. Hence, this is additional evidence that the size of the NPs remains unchanged upon their transfer from the organic to the aqueous phase.

3.3. Conjugation of γ-Fe_2O_3 NPs and PbSe NQDs via Selective Bonding. The formation of the water-soluble nanoparticles, PbSe NQDs funtionalized with amine groups, and γ-Fe_2O_3 NPs functionalized with silicone-oxide ionic groups generated the building blocks for the subsequent hierarchical coupling reaction resulting in the formation of the structurally conjugated fluorescing and magnetic nanoparticles. Figure 5A shows a TEM image of the conjugated structure ensembles of nanoparticles, while Figure 5B exhibits a HR-TEM image of a small domain of the ensembles. This high-resolution image

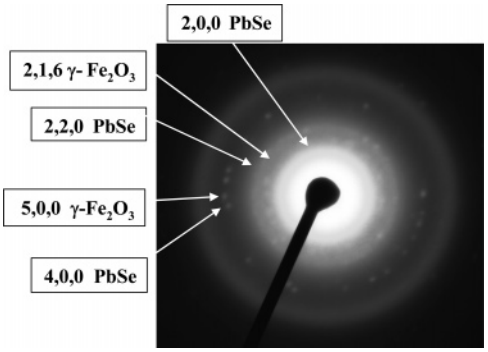

Figure 6. Electron diffraction pattern of the conjugated structure comprised of γ-Fe_2O_3 NPs and PbSe NQDs.

reveals the existence of particles with different lattice fringes (marked by the arrows in the figure) and a common repeating distance of about 1.3 nm. Such a distance is in agreement with the sum of the AET and PSS molecular lengths, as shown schematically in Scheme 3. The schematics describing the hydrogen bonding responsible for the coupling between AET and PSS ligands was obtained from 3-D rendering of energy minimization calculations using commercial programs (see legend for Scheme 3). The hydrogen bonding between AET and PSS occurs via the formation of a pseudo-ring, in which the NH_3^+ group is hydrogen bonded to the lone pairs of the bridged oxygen in PSS and the O^- of PSS is hydrogen bonded to one of the CH_2 groups in AET. Hence, the energetic stabilization in this coupling process is greater than the formation of a simple hydrogen bond.

The electron diffraction pattern of the conjugated structure, shown in Figure 6, is composed of diffraction bands associated with both the magnetic γ-Fe_2O_3 NPs and the semiconductor PbSe NQDs. The assignments of the diffraction rings are labeled in Figure 6, while relevant crystallographic parameters (d-spacing) are summarized in Table 1. Those parameters are in agreement with the known structures; the γ-Fe_2O_3 NP lattice consists of Fe sites with both O_h and T_d symmetries in a relative ratio of 1:0.6 and Fe$-$O bond lengths of 2.094 and 1.876 Å, respectively.[51,52] PbSe NQDs have a perfect ccp/fcc crystal structure.[40]

4. Conclusion

Water-soluble conjugated structures, consisting of magnetic NPs (γ-Fe_2O_3) connected to semiconductor NQDs (PbSe), were synthesized. The NQDs bind to the surface of the magnetic NPs by chemical bonds. The absorbance and PL of the PbSe NQDs showed intense optical transitions of the NQDs in the aqueous solution, retaining the optical properties of the aqueous prepared NQDs in organic medium. In addition, the γ-Fe_2O_3 NPs also exhibit very good morphology and were fully water miscible. Both PbSe NQDs and γ-Fe_2O_3 NPs and the luminescent/magnetic structures (PbSe NQDs/γ-Fe_2O_3 NPs) were characterized using TEM, HR-TEM, XRD, and FTIR. High-resolution TEM images and the electron diffraction patterns confirmed a connection between the magnetic NPs and the PbSe NQDs. This exciting system can be used in a variety of biomedical and

TABLE 1: Crystallographic Parameters of the γ-Fe_2O_3 NPs and PbSe NQDs

radius of diffraction circle (mm)	calculated value of *d* (Å)	*d* of γ-Fe_2O_3 and PbSe phases	*hkl*	nanocrystal
0.65	3.09	3.0	200	PbSe
0.72	2.78	2.78	216	γ-Fe_2O_3
0.92	2.18	2.1	220	PbSe
1.21	1.65	1.67	500	γ-Fe_2O_3
1.28	1.56	1.5	400	PbSe

biological applications. The study of the properties of this system for using it for drug delivery is under investigation.

Acknowledgment. The authors are indebted to Yehudit Schmidt of the Department of Chemical Engineering and the Center of Complex Fluids at the Technion for her assistance with the transmission electron microscopy. The authors are also indebted to Dr. Yong Ding of the School of Materials Science and Engineering at the Georgia Institute of Technology for his assistance with the high-resolution electron microscopy measurements. The authors express their gratitude to the German Israel Foundation (GIF) Contract 156/03-12.6, to the German Israel Program (DIP) Project D 3.2, to the Ministry of Industry, Trade and Labor, Magneton 1000052, to the Russell Berrie foundation for the contribution of excellent infrastructure, and to the donation of Matilda and Gariel Barnett for the establishment of the Nanocrystalline Laboratory at the Technion. This work was also supported in part by the E. and J. Bishop Research Fund and by the National Institutes of Health, through the Centers of Cancer Nanotechnology Excellence Emory GT Nanotechnology Center for Personalized and Predictive Oncology, Award 5-40255-G1: CORE 1.

References and Notes

(1) Klostranec, J. M.; Chan, Warren C. W. *Adv. Mater.* **2006**, *18* (15), 1953.
(2) Lin, Z.; Su, X.; Mu, Y.; Jin, Q. *J. Nanosci. Nanotechnol.* **2004**, *4* (6), 641.
(3) Bukowski, T. J.; Simmons, J. H. *Science* **2002**, *27* (3 and 4), 119.
(4) Tomasulo, M.; Yildiz, I.; Kaanumalle, S. L.; Raymo, F. M. *Langmuir* **2006**, *22* (24), 10284.
(5) Zhang, R.; Wang, X.; Wu, C.; Song, M.; Li, J.; Lv, G.; Zhou, J.; Chen, C.; Dai, Y.; Gao, F.; Fu, D.; Li, X.; Guan, Z.; Chen, B. *Nanotechnology* **2006**, *17* (14), 3622.
(6) Yi, D. K.; Selvan, S. T.; Lee, S. S.; Papaefthymiou, G. C.; Kundaliya, D.; Ying, J. Y. *J. Am. Chem. Soc.* **2005**, *127* (14), 4990.
(7) Koh, I.; Wang, X.; Varughese, B.; Isaacs, L.; Ehrman, S. H.; English, D. S. *J. Phys. Chem. B* **2006**, *110* (4), 1553.
(8) Michalak, L.; Canali, C. M.; Benza, V. G. *Phys. Rev. Lett.* **2006**, *97* (9), 96804/1.
(9) Holzapfel, V.; Lorenz, M.; Weiss, C. K.; Schrezenmeier, H.; Landfester, K.; Mailaender, V. *J. Phys.: Condens. Matter* **2006**, *18* (38), 2581.
(10) Wuang, S. C.; Neoh, K. G.; Kang, E.-T.; Pack, D. W.; Leckband, D. E. *Adv. Funct. Mater.* **2006**, *16* (13), 1723.
(11) Furlani, E. P.; Ng, K. C. *Phys. Rev. E* **2006**, *73* (6), 61919/1.
(12) Gao, X.; Cui, Y.; Levenson, R. M.; Chung, L. W. K.; Nie, S. *Nat. Biotechnol.* **2004**, *22* (8), 969.
(13) Xu, C.; Xu, K.; Gu, H.; Zhong, X.; Guo, Z.; Zheng, R.; Zhang, X.; Xu, B. *J. Am. Chem. Soc.* **2004**, *126* (11), 3392.
(14) Klarreich, E. *Nature* **2001**, *413*, 450.
(15) Clarke, S. J.; Hollmann, C. A.; Zhang, Z.; Suffern, D.; Bradforth, S. E.; Dimitrijevic, N. M.; Minarik, W. G.; Nadeau, J. L. *Nat. Mater.* **2006**, *5*, 409.
(16) Han, M.; Gao, X.; Su, J. Z.; Nie, S. *Nat. Biotechnol.* **2001**, *19*, 631.
(17) Oh, E.; Hong, M.-Y.; Lee, D.; Nam, S.-H.; Yoon, H. C.; Kim, H.-S. *J. Am. Chem. Soc.* **2005**, *127*, 3270.
(18) Shevchenko, E. V.; Talapin, D. V.; Kotov, N. A.; O'Brian, S.; Murray, C. B. *Nature* **2006**, *439* (5), 55.
(19) Wolcott, A.; Gerion, D.; Visconte, M.; Sun, J.; Schwartzberg, A.; Chen, S.; Zhang, J. Z. *J. Phys. Chem. B* **2006**, *110*, 5779.
(20) Wang, D.; He, J.; Rosenzweig, N.; Rosenzweig, Z. *Nano Lett.* **2004**, *4*, 409.
(21) Santoni, A.; Paolucci, G.; Santoro, G.; Prince, K. C.; Christensen, N. E. *J. Phys.: Condens. Matter* **1992**, *4*, 6759.
(22) Alivisatos, A. P. *J. Phys. Chem.* **1996**, *100*, 13226.
(23) Kagan, C. R.; Murray, C. B.; Bawendi, M. G. *Phys. Rev. B* **1996**, *54*, 8633.
(24) Andreev, A. D.; Lipovskii, A. A. *Phys. Rev. B* **1999**, *59*, 15402.
(25) Du, H.; Chen, C.; Krishnan, R.; Krauss, T. D.; Harbold, J. M.; Wise, F. W.; Thomas, M. G.; Silcox, J. *Nano Lett.* **2002**, *2*, 1321.
(26) Wehrenberg, B. L.; Wang, C.; Guyot-Sionnest, P. *J. Phys. Chem. B* **2002**, *106*, 10634.
(27) Schaller, R. D.; Klimov, V. I. *Phys. Rev. Lett.* **2004**, *92*, 186601.
(28) Schaller, R. D.; Petruska, M. A.; Klimov, V. I. *J. Phys. Chem.* **2003**, *107*, 13765.
(29) Klimov, V. I.; Mikhailovsky, A. A.; Xu, S.; Malko, A.; Hollingsworth, J. A.; Leatherdatle, C. A.; Eisler, H. J.; Bawendi, M. G. *Science* **2002**, *290*, 314.
(30) Ellingson, R. J.; Beard, M. C.; Johnson, J. C.; Yu, P.; Micic, O. I.; Nozik, A. J.; Shabaev, A.; Efros, A. L. *Nano Lett.* **2005**, *5*, 865.
(31) Sirota, M.; Galun, E.; Krupkin, V.; Glushko, A.; Kigel, A.; Brumer, M.; Sachshiuk, A.; Amirav, L.; Lifsthiz, E. *Nanophotonic Materials*; Andrews, D. L., Cao, G. C., Gaburro, Z., Eds.; *Proc. SPIE—Int. Soc. Opt. Eng.* **2004**, *5510*, 9.
(32) Steckel, J. S.; Coe-Sullivan, S.; Bulovic, V.; Bawendi, M. G. *Adv. Mater.* **2003**, *15*, 1862.
(33) Gaponik, N.; Radtchenko, I. L.; Gerstenberger, M. R.; Fedutik, Y. A.; Sukhorukov, G. B.; Rogach, A. L. *Nano Lett.* **2003**, *3*, 369.
(34) Sohn, B. H.; Cohen, R. E. *Chem. Mater.* **1997**, *9*, 264.
(35) Sun, S.; Murray, C. B. *J. Magn. Magn. Mater.* **1999**, *85* (8), 4325.
(36) Popplewell, J.; Sakhnini, L. *J. Magn. Magn. Mater.* **1995**, *149*, 72.
(37) Raj, K.; Moskowitz, B.; Casciari, R. *J. Magn. Magn. Mater.* **1995**, *149*, 174.
(38) Molday, R. S.; Mackenzie, D. *J. Immunol. Methods* **1982**, *52*, 353.
(39) Jung, C. W.; Jacobs, P. *Magn. Reson. Imaging* **1995**, *13*, 661.
(40) Yu, W. W.; Falkner, J. C.; Shih, B. S.; Colvin, V. L. *Chem. Mater.* **2004**, *16*, 3318.
(41) Brumer, M.; Kigel, A.; Amirav, L.; Sashchiuk, A.; Solomesch, O.; Tessler, N.; Lifshitz, E. *Adv. Funct. Mater.* **2005**, *15*, 1111.
(42) Larken, E. E.; Grancharov, S. G.; O'Brien, S.; Deming, T. J.; Stucky, G. D.; Murray, C. B.; Held, G. A. *Nano Lett.* **2003**, *3*, 1489.
(43) Frankamp, B. L.; Fischer, N. O.; Hong, R.; Srivastava, S.; Rotello, V. M. *Chem. Mater.* **2006**, *18*, 956.
(44) de Mello, J. C.; Wittmann, H. F.; Friend, R. H. *Adv. Mater.* **1997**, *9*, 230.
(45) Allan, G.; Delerue, C. *Phys. Rev. B* **2004**, *70*, 245321.
(46) Chakraborty, A. K.; Bischoff, K. B.; Astarita, G.; Damewood, J. R., Jr. *J. Am. Chem. Soc.* **1988**, *110*, 6947.
(47) Hyeon, T.; Lee, S. S.; Park, J.; Chung, Y.; Bin, N. H. *J. Am. Chem. Soc.* **2001**, *123*, 12798.
(48) Tannenbaum, R.; Reich, S.; Flenniken, C. L.; Goldberg, E. P. *Adv. Mater.* **2002**, *14* (19), 1402.
(49) Maity, D.; Agrawal, D. C. *J. Magn. Magn. Mater.* **2007**, *308* (1), 46.
(50) Thünemann, A. F.; Schütt, D.; Kaufner, L.; Pison, U.; Möhwald, H. *Langmuir* **2006**, *22*, 2351.
(51) Cornell, R. M.; Schwertmann, U. *The Iron Oxides: Structures, Properties, Reactions, Occurrence, and Uses*, 1st ed.; Wiley-VCH: Weinheim, Germany, 1996.
(52) *X-Ray Identification and Crystal Structures of Clay*; Brown, G., Ed.; The Mineralogical Society of America: Chantilly, VA, 1961.
(53) Frisch, M. J. et al. *Gaussian 98*; Gaussian, Inc.: Pittsburgh, PA, 1998.
(54) *ChemDraw*; Cambridge Soft Corp.: Cambridge, MA.